Inertia-gravity waves in Antarctica: Using ray tracing to study measurements at McMurdo/Scott Base (77.83° S, 166.67° E)

R. Michael Jones[a], Jackson Jandreau[a,b], Xinzhao Chu[a,b]

[a]*Cooperative Institute for Research in Environmental Sciences, University of Colorado, Boulder, Colorado 80309-0216, U.S.A.*
[b]*Department of Aerospace Engineering Sciences, University of Colorado, Boulder, Colorado 80309-0429, U.S.A.*

Abstract

The NOAA/CIRES ray-tracing program is used to learn more about the characteristics of the gravity waves that were inferred from temperature profiles measured with the ground-based LIDAR at McMurdo/Scott Base in Antarctica on 29 June 2011 [Chen et al. 2013, Journal of Geophysical Research: Atmospheres 118 (7), 2794-2808]. The ray-path calculations show that the gravity waves deviate significantly from a great circle path because of wind. The source of the 7.7-hour gravity wave is estimated to be at a height between 55 and 85 km in the atmosphere west of the prime meridian near the coast of Antarctica, but the source could be lower and farther West if it is farther away. Using reverse ray tracing improves the efficiency of estimating the source location of the gravity waves. The usual formula for the acoustic-gravity wave dispersion relation (that depends on only the vertical component of the Earth's angular velocity in the Coriolis force) gives the correct low-frequency cut off, but including all components of the Earth's angular velocity gives more accurate propagation calculations in some cases.

Keywords: gravity waves, Antarctica, ray tracing

1. Introduction

Atmospheric gravity waves perturb the temperature and wind as they propagate. Measuring temperature profiles using LIDAR shows that gravity waves with periods ranging from 3 to 10 hours are typical in Antarctica (Chu et al., 2011; Chen et al., 2013, 2016; Zhao et al., 2017; Chu et al., 2018). Two gravity waves were measured on 29 June 2011 in the height range from 81 km to 107 km above the research station at McMurdo in Antarctica, one gravity wave with a 5.0-hour period and one gravity wave with a 7.7-hour period (Chen et al., 2013).

The 7.7-hour gravity wave had a vertical wavelength of about 22 km, a horizontal wavelength of about 2200 km, a horizontal group speed of about 48 m/s, vertical group speed of about 0.5 m/s upward, propagating in an azimuth direction of about 11° clockwise from north (Chen et al., 2013). Because the group velocity was nearly horizontal, the source was estimated to be in the stratosphere just off the coast of Antarctica near the prime meridian. If the source was in the stratosphere, then it might be a secondary gravity wave produced by primary gravity waves through non-linear processes. (Becker and Vadas, 2018; Vadas et al., 2018).

To illustrate how ray tracing can help give more information about measured gravity waves, we use the CIRES/NOAA ray-tracing program to investigate the 7.7-hour gravity wave.

Section 2 presents the atmospheric temperature and wind profiles used in the calculations. Section 3 describes the appropriate ray-path calculations. Section 4 uses reverse ray tracing to estimate the source location of the gravity waves. Section 5 presents the conclusions.

The appendices show situations where neglecting the horizontal components of the Earth's angular velocity gives ray paths that differ from those that include all components of the Earth's angular velocity when calculating the Coriolis force.

2. The atmospheric model

2.1. Temperature model

As a first approximation to calculate ray paths, we use a temperature profile appropriate to McMurdo, Antarctica for 29 June 2011, 20 UT, as shown in figure 1. The corresponding Brunt-Väisälä frequency profile is shown in figure 2. The temperature profile is very typical in that it clearly shows the troposphere, stratosphere, mesosphere, and thermosphere. Including the spatial variation of the temperature profiles along the path would likely alter the details of the calculations, but would not likely affect the main conclusions.

2.2. Wind model

We have measurements of 7.7-hour gravity waves from 29 June 2011 in the height range of about 80 to 105 km (Chen et al., 2013).

To estimate the source of these gravity waves, we need estimates of the wind in the region of the atmosphere where these gravity waves are propagating. These gravity waves are propagating upward on a nearly horizontal path when they pass McMurdo. Our ray-path calculations show that these waves are above about 73 km during the part of their path over Antarctica. Therefore, we need to model the wind only above about 73 km.

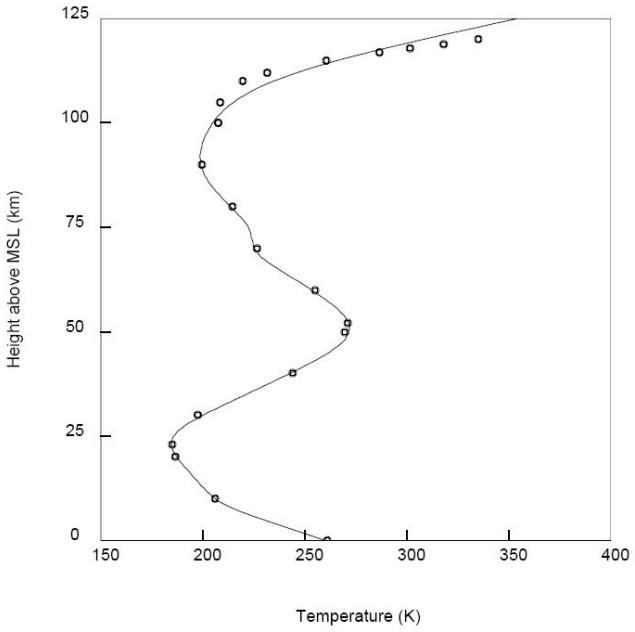

Figure 1: Temperature profile used in the ray path calculations. The circles are from the MSISE-00 model for McMurdo (77.83° S, 166.67° E) for 29 June 2011, 20 UT (NRLMSISE-00, Community Coordinated Modeling Center, 2016). The solid line is our fit to the profile that we used for the ray-path and profile calculations.

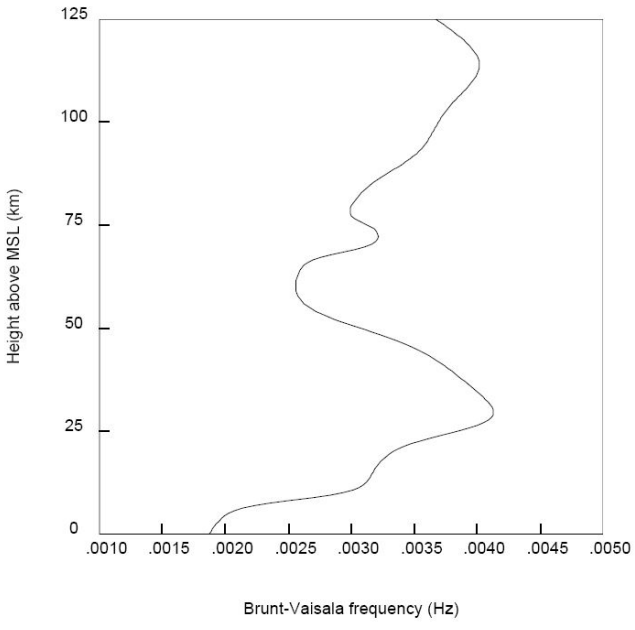

Figure 2: Brunt-Väisälä frequency profile for McMurdo (77.83° S, 166.67° E) for 29 June 2011, 20 UT corresponding to the temperature profile in figure 1.

We have MERRA-2 wind profiles (Gelaro et al., 2017) up to about 73 km that are based on measurements. The best estimates for the wind above 73 km comes from extrapolating the measured profiles above 73 km.

However, the measured wind profiles include gravity-wave-associated components for both the 7.7-hour and the 5.0-hour gravity waves in addition to the background wind profiles. To remove the gravity-wave-associated components, we have time-averaged the wind profiles over a 21-hour period. This averages the wind over about three or four cycles respectively for the 7.7-hour and the 5.0-hour gravity waves.

The resulting time-averaged profiles at a height of about 73 km in the region of the ray paths can be approximated by a clockwise-rotating vortex centered at a latitude of 83° S and a longitude of 285° E. That is the model we are using for our ray-path calculations.

3. Ray-path calculations

The CIRES/NOAA acoustic-gravity wave ray tracing computer program used for these calculations is a general three-dimensional ray tracing program for calculating acoustic-gravity waves in the atmosphere (described in Bedard and Jones, 2013; Jones and Bedard, 2015, 2018) based on an earlier program HARPA for calculating the propagation of acoustic waves (Jones et al., 1986a,b; Georges et al., 1990). The ray tracing program calculates ray paths by integrating Hamilton's equations in Earth-centered spherical polar coordinates (Jones et al., 1986a, pp. 89-91).

Many gravity waves (including the 7.7-hour gravity wave studied here) are in the category of asymptotic gravity waves, that have a wave-normal direction that is at an angle of $\cos^{-1} \omega_i/N$ from the horizontal, where ω_i is the intrinsic frequency (the frequency in a frame moving with the wind) and N is the Brunt-Väisälä frequency. The wave frequency of a gravity wave with a period of 7.7 hours is so low that wave-normal directions would be within a degree or so of vertical, and the corresponding ray directions would be nearly horizontal. In addition, as is well known, the vertical component of the wave-normal direction is in the opposite direction from the vertical component of the ray direction. Because Chen et al. (2013) observed the wave fronts of the 7.7 hour gravity wave to be moving downward, we calculate here ray paths for gravity waves in which the wave-normal elevation angle is about $-89°$ (that is, down) with ray directions nearly horizontal, but moving slightly up.

To correctly interpret gravity wave measurements at such low frequencies with ray tracing calculations requires an accurate representation of the effect of Coriolis force on the propagation. Although the usual dispersion relation (Eckart, 1960, eq. (51-2), p. 125) (Gossard and Hooke, 1975, eq. (23-7), p. 112) that includes the effect of only the vertical component of the Earth's angular velocity on the Coriolis force[1] gives the correct low-frequency cut off for inertial gravity waves, it neglects

[1] sometimes referred to as the "Shallow atmosphere" approximation (Phillips, 1966; Hickey and Cole, 1987)

possibly significant effects from the horizontal components of the Earth's angular velocity. The appendices show situations where neglecting the horizontal components of the Earth's angular velocity gives ray paths that differ from those that include all components of the Earth's angular velocity.

4. Reverse ray tracing

The most efficient way to search for the source of the gravity waves observed at McMurdo is to use reverse ray tracing. That is, we start a gravity wave at McMurdo and send it back toward the direction it was seen coming from. To correctly do reverse ray tracing requires that the wind direction is reversed everywhere, which we have done. We assume the source is very far away, so we neglect the curvature of the wave front. That is, we assume that the horizontal wavelength is independent of height, but the vertical wavelength will vary with height.

The 7.7-hour gravity waves were measured to come from an azimuth direction of about 11° clockwise from north (Chen et al., 2013). To find out the elevation angle of the gravity waves as they pass over McMurdo, we use the information that the vertical wavelength for the gravity waves was measured to be about 22 km (Chen et al., 2013). We adjusted the elevation angle of the gravity wave at various heights until we got the vertical wavelength profile shown in figure 3, which shows the vertical wavelength profile above McMurdo Station for a gravity wave that has wave-normal direction of 11° clockwise from north and −89.56° from horizontal at a height of 80 km and −89.655° from horizontal at a height of 105 km. The average vertical wavelength over this height range is about 22 km, which is the vertical wavelength measured for the 7.7-hour gravity wave at McMurdo on 29 June 2011 (Chen et al., 2013).

From that information, we launched rays from heights of 80 km and 105 km above McMurdo station back in the direction they seemed to be coming from. Figure 4 shows a projection of those ray paths on a vertical plane, and figure 5 shows a projection of those ray paths on a map of Antarctica. The heights of 80 km and 105 km of the gravity waves as they pass over McMurdo represent the height range of the gravity waves observed over McMurdo on 29 June 2011 (Chen et al., 2013). Figure 4 shows that the height of those gravity waves at the source would be between about 55 and 85 km, or ever lower if the gravity waves came from farther away. Figure 5 shows that the source of the gravity waves would be roughly about 10° or 20° west of the prime meridian, or even farther west if the source is farther away.

Because figures 4 and 5 include spatially varying wind profiles that approximate the actual (time-averaged) wind profiles (extrapolated upward), they probably give the most accurate estimate for the source of the measured 7.7-hour gravity wave.

5. Conclusions

We made ray-path calculations and wavelength profile calculations for the 7.7-hour gravity wave that was observed at McMurdo, Antarctica on 29 June 2011.

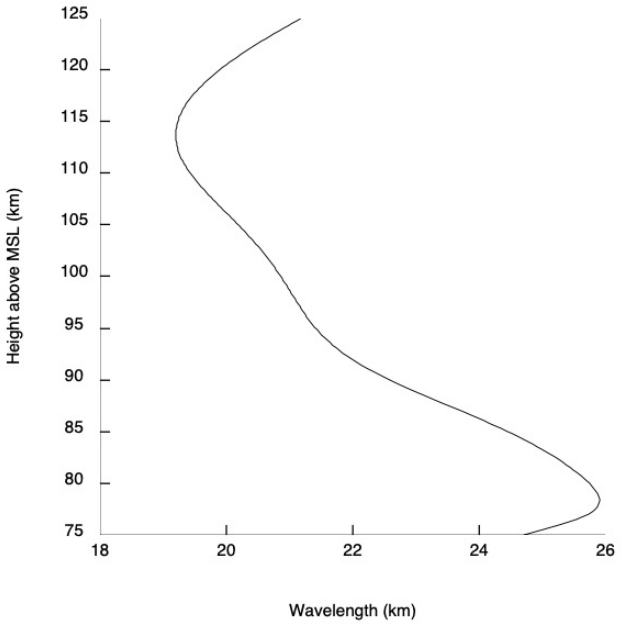

Figure 3: Vertical wavelength profile above McMurdo Station for a wave-normal direction of 11° clockwise from north and −89.56° from horizontal at a height of 80 km and −89.655° from horizontal at a height of 105 km. The average vertical wavelength over this height range is about 22 km. The horizontal wavelength is independent of height and is about 3360 km.

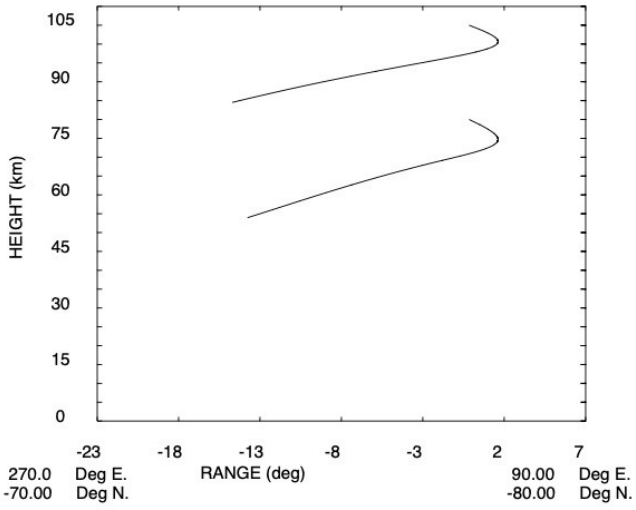

Figure 4: Projection of the reverse ray paths on the vertical plane through the 90° and 270° meridians. The heights of the gravity waves over McMurdo are 80 and 105 km. The heights of the gravity waves near the possible source are about 55 and 85 km. The wave-normal direction of the reversed gravity waves over McMurdo is 191° in azimuth and 89.56° in elevation at 80 km and 89.655° in elevation at 105 km.

Figure 5: Projection on the ground of the reverse ray paths in figure 4. The wind is represented by a vortex centered at a latitude of 83° S and a longitude of 285° E, indicated by the center of the circle. The wind speed on the circle is 30 m/s. The ray paths are superimposed on a map of Antarctica.

Our most accurate estimates of the source for the 7.7-hour gravity wave is west of the prime meridian and at heights between about 55 and 85 km if the source is near the coast of Antarctica, as shown in figures 4 and 5. However, if the source is farther away, then it would be lower and more to the West. These estimates are to the west of the estimates given by Chen et al. (2013), which did not account for the deviation of the gravity waves from a great-circle path caused by the wind.

Although the gravity wave was measured in the height range of 80 km up to 105 km, the gravity wave may have extended lower, maybe even to the ground. If so, then the source could have been anywhere from the ground up to 85 km.

Because there can be significant differences in both ray paths and vertical-wavelength profiles between dispersion relations that include or neglect the horizontal components of the Earth's angular velocity in the Coriolis terms, it is advisable to include all components of the Earth's angular velocity when calculating Coriolis effects on gravity-wave propagation.

Acknowledgments

This research was partially supported by the National Science Foundation (NSF) grants PLR-1246405 and AGS-1136272.

Appendix A. The usual dispersion relation ignores horizontal components of the Earth's angular velocity

The usual barotropic approximation to the acoustic-gravity wave dispersion relation is (Eckart, 1960, eq. (51-2), p. 125) (Gossard and Hooke, 1975, eq. (23-7), p. 112) (Jones, 2006, equation (1)):

$$(k_x^2 + k_y^2)(N^2 - \omega^2) - (\omega^2 - 4\Omega_z^2)(k_z^2 + \mathbf{k}_A^2 - \frac{\omega^2}{C^2}) = 0\,, \quad \text{(A.1)}$$

where N is the Brunt-Väisälä frequency, $\omega = \sigma - \mathbf{k}\cdot\mathbf{U}$ is the intrinsic frequency, σ is the wave frequency, $\mathbf{U}$ is the background fluid velocity, $\mathbf{k}$ is the wavenumber, k_z is its vertical component, k_x and k_y are its horizontal components, Ω_z is the vertical component of the Earth's angular velocity, C is sound speed, and $\mathbf{k}_A \equiv \nabla\rho/(2\rho)$, where ρ is density.

Because the main Coriolis effect on the propagation of gravity waves is to give a low-frequency cutoff, and because that cutoff is correctly given by an approximation that neglects the effects of the horizontal components of the Earth's angular velocity, it made sense to use the simpler formula (A.1) based on that approximation before the wide-spread use of computers to make calculations. However, when making calculations with a computer, there is less advantage of a simple formula if a more accurate formula can give better results.

Appendix B. Including all components of the Earth's angular velocity in the Coriolis effect for the dispersion relation

Eckart (1960, sections 37-38, pp. 94-101) considers the horizontal components of the Earth's angular velocity and gives

the appropriate equations, but does not calculate a dispersion relation that includes the horizontal components. Gossard and Hooke (1975, section 10, p. 50) also consider the possibility of including the horizontal components of the Earth's angular velocity in the Coriolis effect on the dispersion relation, but decide that the effect would be small. Jones (2006, equation (5)) gives a general formula for the acoustic-gravity-wave dispersion relation, including baroclinicity, rate-of-strain, and the Coriolis force (including all components of the Earth's angular velocity).

Equation (D.7), which gives an approximate dispersion relation that neglects rate-of-strain and baroclinicity, but still includes the effects of all components of the Earth's angular velocity on the Coriolis force, can be written

$$(\mathbf{k}^2 + \mathbf{k}_A^2)(N^2 - \omega^2) - \left(k_z^2 + k_A^2\right)N^2 + 4(\mathbf{k}_A \cdot \tilde{\mathbf{\Omega}})^2 + 4(\mathbf{k} \cdot \tilde{\mathbf{\Omega}})^2 + 4\omega\tilde{\mathbf{\Omega}} \times \mathbf{\Gamma} \cdot \mathbf{k} + 1/C^2(\omega^4 - 4\omega^2\tilde{\mathbf{\Omega}}^2) = 0\,, \quad \text{(B.1)}$$

where $\tilde{\mathbf{\Omega}} = \mathbf{\Omega} + \zeta/4$, $\zeta = \nabla \times \mathbf{U}$ is vorticity, and $\mathbf{\Omega}$ is the Earth's angular velocity.

Although the main Coriolis term (the first Coriolis term) in (B.1) agrees with the corresponding term in (A.1), other Coriolis terms in (B.1) differ because they depend on the horizontal components of the Earth's angular velocity.

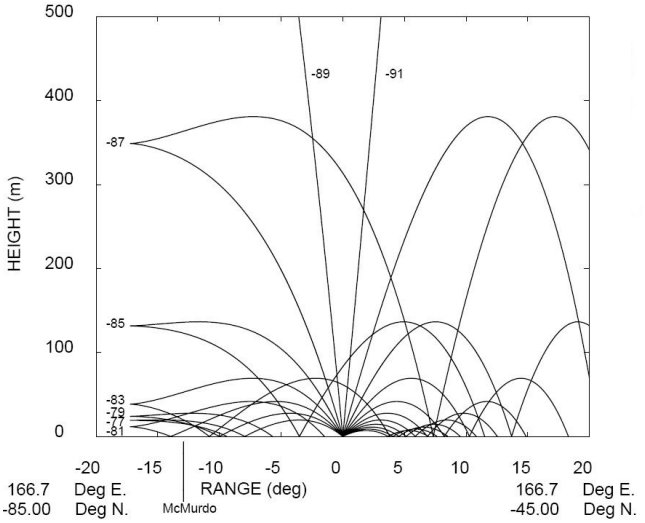

Figure C.6: Ray paths in the North-South plane neglecting horizontal components of the Earth's angular velocity for the Coriolis force in the dispersion relation. The source is on the ocean surface at a latitude of 65° South and a longitude of 166.67° East. The frequency is 23 μHz. The elevation angles of transmission (wave-normal direction) of the various rays are indicated in the figure, and are relative to propagation to the South. Negative elevation angles for the wave-normal direction correspond to upward ray propagation for gravity waves. McMurdo (as indicated in the figure) is located 12.83° South of the source.

Appendix C. Comparison

To compare ray paths calculated using the usual approximation (A.1) with the dispersion relation that includes Coriolis effects from all components of the Earth's angular velocity (B.1), we use a temperature profile appropriate to McMurdo, Antarctica for 29 June 2011, 20 UT, as shown in figure 1. The corresponding Brunt-Väisälä frequency profile is shown in figure 2.

Figure C.6 shows the ray paths in the North-South plane neglecting horizontal components of the Earth's angular velocity using the usual dispersion relation (A.1). Figure C.7 shows the corresponding ray paths using the dispersion relation that includes Coriolis effects from all components of the Earth's angular velocity (B.1). As can be seen, the rays are turned back at the same latitude in both figures C.6 and C.7, indicating that the low-frequency cut off for gravity waves depends only on the vertical component of the Earth's angular velocity. However, the ray paths in the two figures differ significantly, indicating that accurate calculation of ray paths requires including all components of the Earth's angular velocity in the dispersion relation.

In addition to comparing ray paths for the two versions of the dispersion relation, we can also compare profiles of vertical wavenumber and vertical wavelength. Figures C.8 and C.9 show a comparison of vertical-wavenumber profiles for the two versions of the dispersion relation. That they differ significantly is clear. Figures C.10 and C.11 show a comparison of vertical-wavelength profiles for the two versions of the dispersion relation. That they differ significantly is also clear. Figures C.12 and C.13 show a comparison of vertical-wavelength profiles for the two versions of the dispersion relation for a different elevation angle at the ground.

Because of horizontal gradients caused by the latitude-dependence of the Coriolis terms, there is not a one-to-one correspondence between the raypaths in figures C.6 and C.7 with the profiles in figures C.8 through C.13. However, both ray-path plots and profiles show that the turning-point height increases with elevation angle and that the turning-point heights for the dispersion relation that includes all components of the Earth's angular velocity are higher than those when the effect of the horizontal components of the Earth's angular velocity are neglected.

Although the examples presented here do not include wind, the results are similar when wind is included.

Appendix D. Dispersion relation including all components of the Earth's angular velocity

Jones (2006, equation (5)) gives a general formula for the acoustic-gravity wave dispersion relation, including baroclinicity, rate-of-strain, and all components of the Earth's angular velocity on the Coriolis force. However, we start with (Jones, 2006, equation (10)), which neglects rate of strain in the dispersion relation as a special case of the general dispersion relation.

$$(\mathbf{k}^2 + \mathbf{k}_A^2)(N^2 - \omega^2) + \mathbf{k} \cdot \mathbf{S} \cdot \mathbf{k} + \mathbf{k}_A \cdot \mathbf{S} \cdot \mathbf{k}_A + \mathbf{A} \cdot \mathbf{k} + 1/C^2(\omega^4 - 4\omega^2\tilde{\mathbf{\Omega}}^2 + B^2/2 - 2i\omega\tilde{\mathbf{\Omega}} \cdot \mathbf{B}) = 0\,, \quad \text{(D.1)}$$

where N is the Brunt-Väisälä frequency[2], $\mathbf{g}$ is the acceleration due to gravity, $\omega = \sigma - \mathbf{k} \cdot \mathbf{U}$ is the intrinsic frequency, σ is

[2]The Brunt-Väisälä frequency, N, is calculated from $N^2 = \nabla\tilde{\rho}_{\text{pot}} \cdot \tilde{\mathbf{g}}/\rho =$

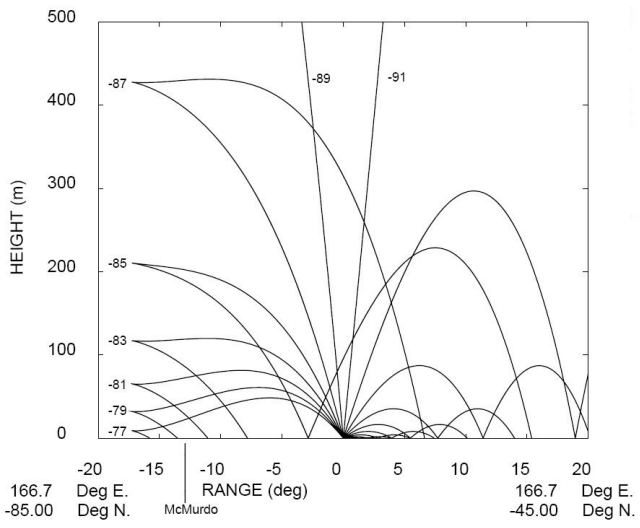

Figure C.7: Ray paths in the North-South plane including all components of the Earth's angular velocity for the Coriolis force in the dispersion relation. Otherwise, conditions are as in figure C.6.

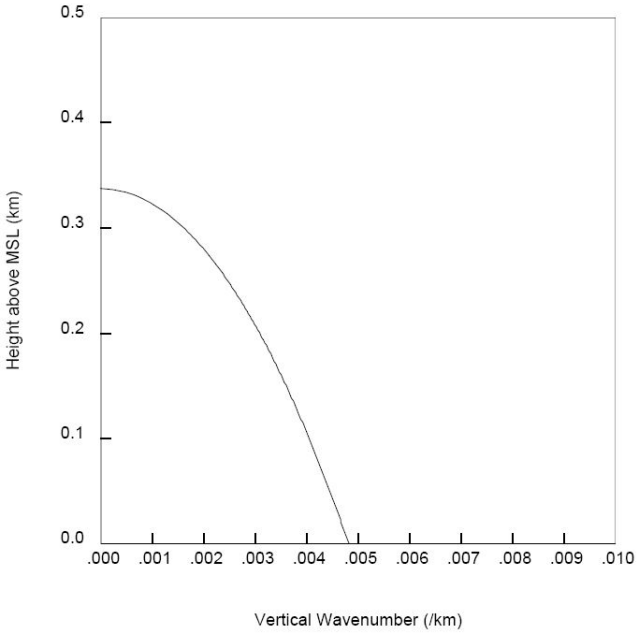

Figure C.8: Vertical-wavenumber profile at McMurdo (77.83° S, 166.67° E) neglecting horizontal components of the Earth's angular velocity for the Coriolis force in the dispersion relation. The frequency is 23 μHz. Propagation is toward the South. The elevation angle at the ground is −88.7°. The wave is evanescent above the turning point, the height where the wavenumber is equal to zero.

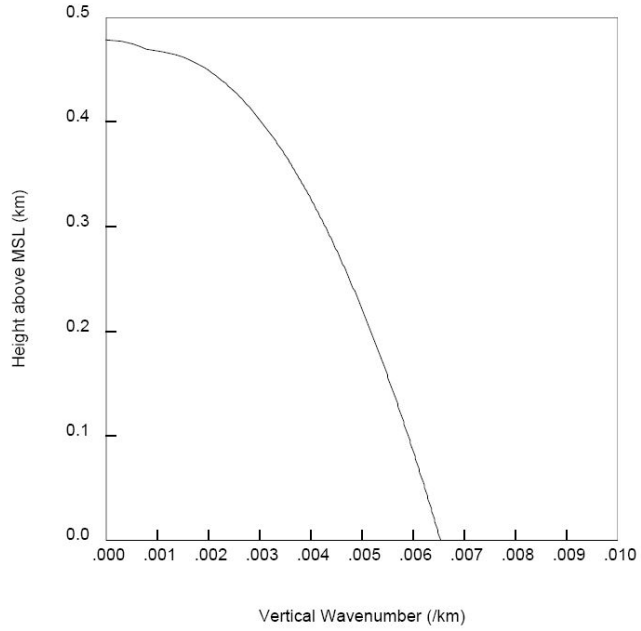

Figure C.9: Vertical-wavenumber profile at McMurdo including all components of the Earth's angular velocity for the Coriolis force in the dispersion relation. The elevation angle at the ground is −88.7°. Otherwise, conditions are as in figure C.8.

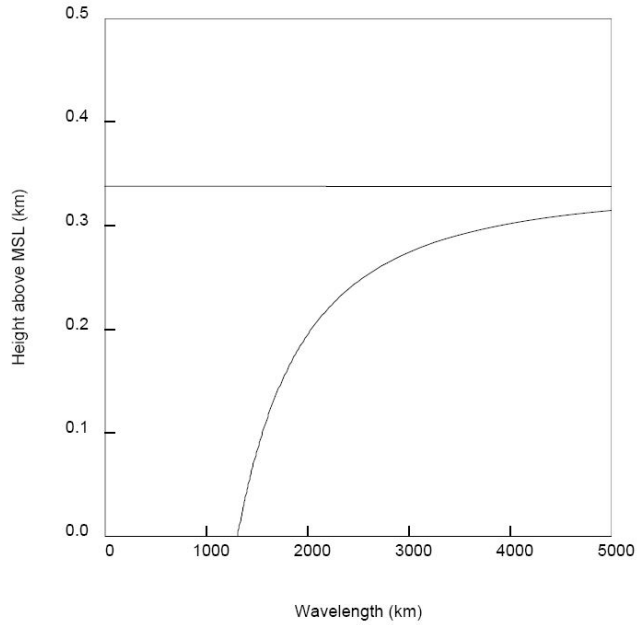

Figure C.10: Vertical-wavelength profile at McMurdo neglecting horizontal components of the Earth's angular velocity for the Coriolis force in the dispersion relation. The elevation angle at the ground is −88.7°. Otherwise, conditions are as in figure C.8. Because the vertical wavelength is proportional to the inverse of the vertical wavenumber, the vertical wavelength diverges at the turning point, as can be seen.

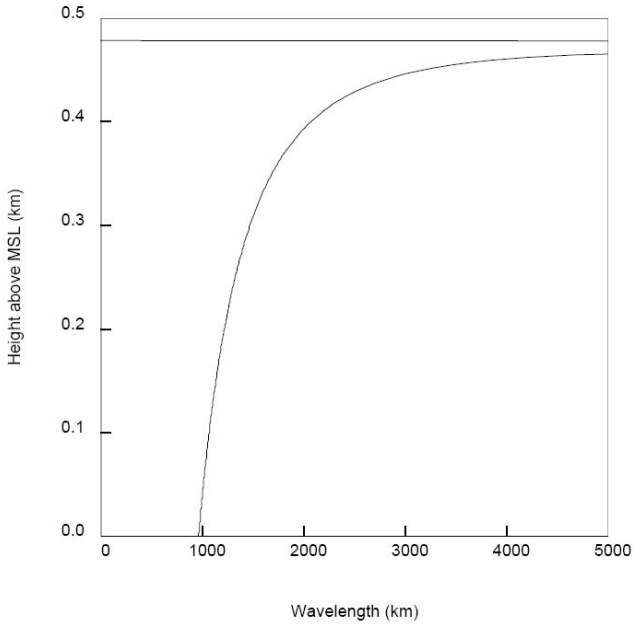

Figure C.11: Vertical-wavelength profile at McMurdo including all components of the Earth's angular velocity for the Coriolis force in the dispersion relation. The elevation angle at the ground is −88.7°. Otherwise, conditions are as in figure C.8.

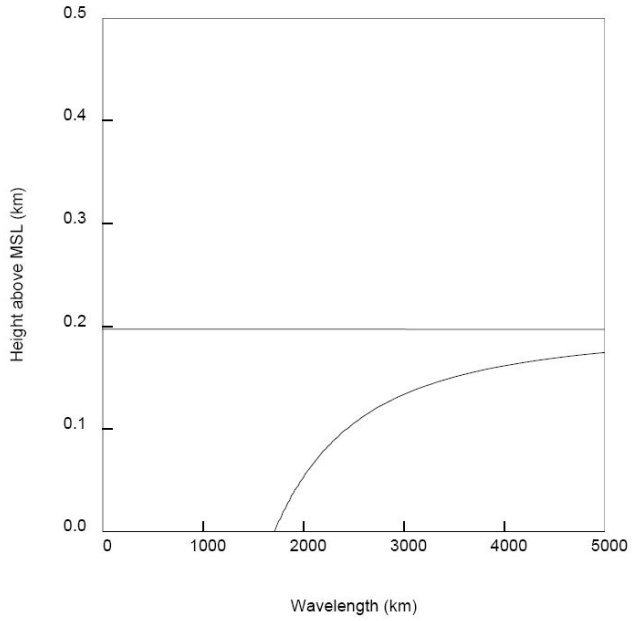

Figure C.12: Vertical-wavelength profile at McMurdo neglecting horizontal components of the Earth's angular velocity for the Coriolis force in the dispersion relation. The elevation angle at the ground is −88.3°. Otherwise, conditions are as in figure C.8.

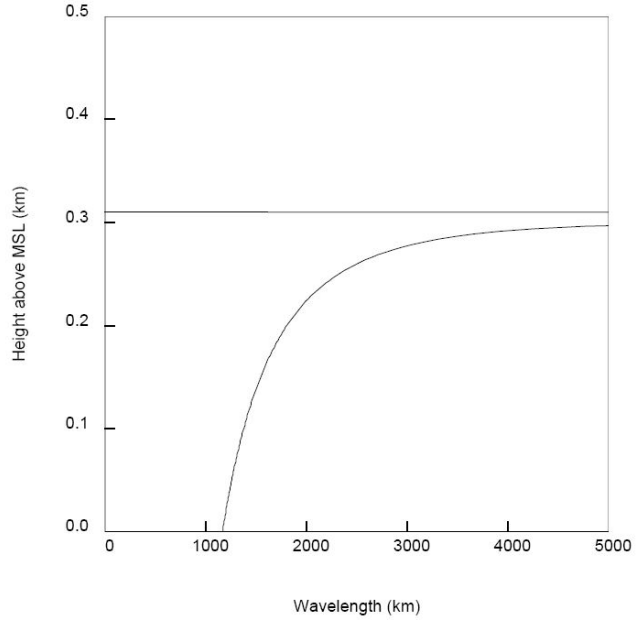

Figure C.13: Vertical-wavelength profile at McMurdo including all components of the Earth's angular velocity for the Coriolis force in the dispersion relation. The elevation angle at the ground is −88.3°. Otherwise, conditions are as in figure C.8.

the wave frequency, $\mathbf{U}$ is the background fluid velocity, $\mathbf{k}$ is the wavenumber, $\mathbf{B}$ is the baroclinic vector, $\tilde{\mathbf{\Omega}} = \mathbf{\Omega} + \zeta/4$, where $\zeta = \nabla \times \mathbf{U}$ is vorticity, $\mathbf{\Omega}$ is the Earth's angular velocity, C is sound speed, $\mathbf{k}_A \equiv \nabla\rho/(2\rho)$, where ρ is density, $\mathbf{S}$ is the symmetric matrix defined by

$$S_{\alpha\beta} = \underbrace{-\frac{1}{2\rho}\left(\frac{\partial\tilde{\rho}_{pot}}{\partial x_\alpha}\tilde{g}_\beta + \frac{\partial\tilde{\rho}_{pot}}{\partial x_\beta}\tilde{g}_\alpha\right)}_{1} \underbrace{+4\tilde{\Omega}_\alpha\tilde{\Omega}_\beta}_{2} \underbrace{+\frac{i}{\omega}\left(\tilde{\Omega}_\alpha B_\beta + \tilde{\Omega}_\beta B_\alpha\right)}_{3} , \tag{D.2}$$

$\tilde{\mathbf{g}} \equiv \nabla p/\rho = \mathbf{g} - D\mathbf{U}/Dt - 2\mathbf{\Omega} \times \mathbf{U}$ is the effective vector acceleration due to gravity [including (minus) the acceleration of the background flow], $\tilde{\rho}_{pot}$ is local potential density, defined by $\nabla\tilde{\rho}_{pot} = \nabla\rho - \nabla p/C^2$ (Jones, 2005, 2008a), p is pressure,

$$\mathbf{A} = (4\omega\tilde{\mathbf{\Omega}} + i\mathbf{B}) \times \mathbf{\Gamma} + 2\mathbf{k}_A \cdot \tilde{\mathbf{\Omega}}\mathbf{B}/\omega , \tag{D.3}$$

and $\mathbf{\Gamma} = \mathbf{k}_A - \tilde{\mathbf{g}}/C^2$ is the vector generalization Jones (2001, 2012) of Eckart's coefficient (Gossard and Hooke, 1975, p. 90).

Term 2 in (D.2) is a Coriolis term, which we will be keeping. Term 3 in (D.2) is a baroclinic and Coriolis term, which we shall be neglecting when we neglect baroclinic terms.

Neglecting the baroclinic terms in (D.1), (D.2), and (D.3) gives

$$(\mathbf{k}^2 + \mathbf{k}_A^2)(N^2 - \omega^2) + \mathbf{k} \cdot \mathbf{S} \cdot \mathbf{k} + \mathbf{k}_A \cdot \mathbf{S} \cdot \mathbf{k}_A + \mathbf{A} \cdot \mathbf{k} + 1/C^2(\omega^4 - 4\omega^2\tilde{\mathbf{\Omega}}^2) = 0 , \tag{D.4}$$

$(\nabla\rho - \nabla p/C^2) \cdot \tilde{\mathbf{g}}/\rho$, where $\tilde{\rho}_{\rm pot}$ is local potential density, p is pressure, C is sound speed, $\tilde{\mathbf{g}} = \nabla p/\rho$ is the effective acceleration due to gravity

where **S** is the symmetric matrix defined by

$$S_{\alpha\beta} = \underbrace{-\frac{1}{2\rho}\left(\frac{\partial\tilde{\rho}_{pot}}{\partial x_\alpha}\tilde{g}_\beta + \frac{\partial\tilde{\rho}_{pot}}{\partial x_\beta}\tilde{g}_\alpha\right)}_{1} \underbrace{+4\tilde{\Omega}_\alpha\tilde{\Omega}_\beta}_{2} , \tag{D.5}$$

and

$$\mathbf{A} = 4\omega\tilde{\mathbf{\Omega}} \times \mathbf{\Gamma} . \tag{D.6}$$

Substituting (D.5) and (D.6) into (D.4) gives

$$\begin{aligned}(\mathbf{k}^2 + \mathbf{k}_A^2)(N^2 - \omega^2) - \tfrac{1}{\rho}\mathbf{k}\cdot\nabla\tilde{\rho}_{pot}\,\tilde{\mathbf{g}}\cdot\mathbf{k} - \tfrac{1}{\rho}\mathbf{k}_A\cdot\nabla\tilde{\rho}_{pot}\,\tilde{\mathbf{g}}\cdot\mathbf{k}_A \\ +4(\mathbf{k}\cdot\tilde{\mathbf{\Omega}})^2 + 4(\mathbf{k}_A\cdot\tilde{\mathbf{\Omega}})^2 + 4\omega\tilde{\mathbf{\Omega}}\times\mathbf{\Gamma}\cdot\mathbf{k} \\ +1/C^2(\omega^4 - 4\omega^2\tilde{\mathbf{\Omega}}^2) = 0\end{aligned} \tag{D.7}$$

for the acoustic-gravity-wave dispersion relation in which all components of the Earth's angular velocity are included in the Coriolis terms.

References

Becker, E., Vadas, S. L., 2018. Secondary gravity waves in the winter mesosphere: Results from a high-resolution global circulation model. Journal of Geophysical Research: Atmospheres 123 (5), 2605–2627.

Bedard, Jr., A. J., Jones, R. M., 2013. Infrasonic ray tracing applied to mesoscale atmospheric structures: Refraction by hurricanes. J. Acoust. Soc. Am. 134 (5), 3446–3451.

Chen, C., Chu, X., McDonald, A. J., Vadas, S. L., Yu, Z., Fong, W., Lu, X., 2013. Inertia-gravity waves in antarctica: A case study using simultaneous lidar and radar measurements at McMurdo/Scott Base (77.8°S, 166.7°E). Journal of Geophysical Research: Atmospheres 118 (7), 2794–2808.
URL http://dx.doi.org/10.1002/jgrd.50318

Chen, C., Chu, X., Zhao, J., Roberts, B. R., Yu, Z., Fong, W., Lu, X., Smith, J. A., 2016. Lidar observations of persistent gravity waves with periods of 3-10 h in the Antarctic middle and upper atmosphere at McMurdo (77.83°S, 166.67°E). Journal of Geophysical Research: Space Physics 121 (2), 1483–1502, 2015JA022127.
URL http://dx.doi.org/10.1002/2015JA022127

Chu, X., Yu, Z., Gardner, C. S., Chen, C., Fong, W., 2011. Lidar observations of neutral Fe layers and fast gravity waves in the thermosphere (110-155 km) at McMurdo (77.8°S, 166.7°E), antarctica. Geophysical Research Letters 38 (23), L23807.
URL http://dx.doi.org/10.1029/2011GL050016

Chu, X., Zhao, J., Lu, X., Harvey, V. L., Jones, R. M., Chen, C., Fong, W., Yu, Z., Roberts, B. R., Dörnbrack, A., 2018. Lidar observations of stratospheric gravity waves from 2011 to 2015 at McMurdo (77.84°S, 166.69°E), Antarctica: 2. Potential energy densities, lognormal distributions, and seasonal variations. Journal of Geophysical Research: Atmospheres 123 (15), 7910–7934.

Eckart, C., 1960. Hydrodynamics of Oceans and Atmospheres. Pergamon Press, Oxford.

Gelaro, R., McCarty, W., Suárez, M. J., Todling, R., Molod, A., Takacs, L., Randles, C. A., Darmenov, A., Bosilovich, M. G., Reichle, R., Wargan, K., Coy, L., Cullather, R., Draper, C., Akella, S., Buchard, V., Conaty, A., da Silva, A. M., Gu, W., Kim, G.-K., Koster, R., Lucchesi, R., Merkova, D., Nielsen, J. E., Partyka, G., Pawson, S., Putman, W., Rienecker, M., Schubert, S. D., Sienkiewicz, M., Zhao, B., 2017. The modern-era retrospective analysis for research and applications, version 2 (merra-2). Journal of Climate 30 (14), 5419 – 5454.
URL https://journals.ametsoc.org/view/journals/clim/30/14/jcli-d-16-0758.1.xml

Georges, T. M., Jones, R. M., Lawrence, R. S., 1990. A PC version of the HARPO ocean acoustic ray-tracing program. Tech. Memo ERL WPL-180, Natl. Oceanic and Atmos. Admin., Boulder, Colorado, 18 pp. (program available at http://cires.colorado.edu/~mjones/raytracing/programs.htm).

Gossard, E. E., Hooke, W. H., 1975. Waves in the Atmosphere. Elsevier Scientific Publishing Company, Amsterdam.

Hickey, M., Cole, K., 1987. A quartic dispersion equation for internal gravity waves in the thermosphere. Journal of Atmospheric and Terrestrial Physics 49 (9), 889 – 899, http://dx.doi.org/10.1016/0021-9169(87)90003-1.

Jones, R. M., 2001. The dispersion relation for internal acoustic-gravity waves in a baroclinic fluid. Physics of Fluids 13, 1274–1280, errata available at (Jones, 2012, http://cires.colorado.edu/~mjones/pubs/errata9.pdf, date last viewed 4 April 2018).

Jones, R. M., November 2005. A general dispersion relation for internal gravity waves in the atmosphere or ocean, including baroclinicity, vorticity, and rate of strain. J. Geophys. Res. 110, D22106, doi: 10.1029/2004JD005654, Errata available at (Jones, 2008a, http://cires.colorado.edu/~mjones/pubs/errata7.pdf, date last viewed 4 April 2018).

Jones, R. M., November 2006. Minimum and maximum propagation frequencies for internal gravity waves. J. Geophys. Res. 111, D06109, doi: 10.1029/2005JD006189, Errata available at (Jones, 2008b, http://cires.colorado.edu/~mjones/pubs/errata8.pdf, date last viewed 4 April 2018).

Jones, R. M., 2008a. Errata: A general dispersion relation for internal gravity waves in the atmosphere or ocean, including baroclinicity, vorticity, and rate of strain, *J. Geophys. Res.*, 2005, doi: 10.1029/2004JD005654, Errata available at http://cires.colorado.edu/~mjones/pubs/errata7.pdf (date last viewed 4 April 2018).

Jones, R. M., 2008b. Errata: Minimum and maximum propagation frequencies for internal gravity waves, *J. Geophys. Res.*, 2006, doi: 10.1029/2005JD006189, Errata available at http://cires.colorado.edu/~mjones/pubs/errata8.pdf (date last viewed 4 April 2018).

Jones, R. M., 2012. Errata: The dispersion relation for internal acoustic-gravity waves in a baroclinic fluid, *Physics of Fluids*, 2001, 1274-1280, Errata available at http://cires.colorado.edu/~mjones/pubs/errata9.pdf (date last viewed 4 April 2018).

Jones, R. M., Bedard, Jr., A. J., 2015. Infrasonic ray tracing applied to small-scale atmospheric structures: Thermal plumes and updrafts/downdrafts. J. Acoust. Soc. Am. 137 (2), 625–632.

Jones, R. M., Bedard, Jr., A. J., 2018. Atmospheric gravity wave ray tracing: Ordinary and extraordinary waves. Journal of Atmospheric and Solar-Terrestrial Physics 179, 342 – 357.

Jones, R. M., Riley, J. P., Georges, T. M., 1986a. HARPA - A versatile three-dimensional Hamiltonian ray-tracing program for acoustic waves in the atmosphere above irregular terrain. NOAA Special Report, GovDoc No. C55.602:H 18; GPO Item No. 207-C-1; PB87132031, National Oceanic and Atmospheric Administration, Boulder, Colorado, 410 pp., report available at http://cires.colorado.edu/~mjones/pubs/harpa.pdf (date last viewed 4 April 2018), program available at http://cires.colorado.edu/~mjones/raytracing (date last viewed 4 April 2018).

Jones, R. M., Riley, J. P., Georges, T. M., 1986b. HARPO - A versatile three-dimensional Hamiltonian ray-tracing program for acoustic waves in an ocean with irregular bottom. NOAA Special Report, GovDoc No. C55.602:H 23; GPO Item No. 0207-C-01; PB87172573, National Oceanic and Atmospheric Administration, Boulder, Colorado, 455 pp., report available at http://cires.colorado.edu/~mjones/pubs/harpo.pdf (date last viewed 4 April 2018), program available at http://cires.colorado.edu/~mjones/raytracing (date last viewed 4 April 2018).

NRLMSISE-00, Community Coordinated Modeling Center, 2016. NRLMSISE-00 Atmosphere Model, http://ccmc.gsfc.nasa.gov/modelweb/models/nrlmsise00.php.

Phillips, N. A., 1966. The equations of motion for a shallow rotating atmosphere and the "traditional approximation". Journal of the Atmospheric Sciences 23 (5), 626–628, doi:10.1175/1520-0469(1966)023<0626:TEOMFA>2.0.CO;2.

Vadas, S. L., Zhao, J., Chu, X., Becker, E., 2018. The excitation of secondary gravity waves from local body forces: Theory and observation. Journal of Geophysical Research: Atmospheres 123 (17), 9296–9325.

Zhao, J., Chu, X., Chen, C., Lu, X., Fong, W., Yu, Z., Jones, R. M., Roberts, B. R., Dörnbrack, A., 2017. Lidar observations of stratospheric gravity

waves from 2011 to 2015 at McMurdo (77.84°S, 166.69°E), Antarctica: 1. Vertical wavelengths, periods, and frequency and vertical wave number spectra. Journal of Geophysical Research: Atmospheres 122 (10), 5041–5062, 2016JD026368.
URL http://dx.doi.org/10.1002/2016JD026368